ADVANCED ENERGY MATERIALS

Supporting Information

for *Adv. Energy Mater.,* DOI: 10.1002/aenm.202102283

How Does the Creep Stress Regulate Void Formation at the Lithium-Solid Electrolyte Interface during Stripping?

Hanghang Yan, Karnpiwat Tantratian, Kevin Ellwood, Elisa T. Harrison, Mark Nichols, Xiangyang Cui, and Lei Chen**

Supporting Information

How does the creep stress regulate void formation at the lithium-solid electrolyte interface during stripping?

Hanghang Yan, Karnpiwat Tantratian, Kevin Ellwood, Elisa T. Harrison, Mark Nichols, Xiangyang Cui, and Lei Chen**

H. Yan, Prof. X. Cui
State Key Laboratory of Advanced Design and Manufacturing for Vehicle Body
Hunan University
Changsha 410082, PR China
E-mail: cuixy@hnu.edu.cn

K. Tantratian, Dr. L. Chen
Department of Mechanical Engineering
University of Michigan-Dearborn
48128-1491 Dearborn, Michigan, United States.
E-mail: leichn@umich.edu

Dr. K. Ellwood, Dr. E. Harrison, Dr. M. Nichols
Research and Innovation Center
Ford Motor Company
48121 Dearborn, Michigan, United States

S1. Creep/contact electro-chemo-mechanical model

This section presents the detailed derivation of the creep/contact model. The model can be divided into three parts: Li^+ transport in solid electrolyte (SE), creep stress in Lithium (Li) metal, and linking Li^+ transport and creep stress of Li metal. The governing equations of the creep/contact model are summarized in **Figure S2**.

S1.1 Li^+ transport in SE

The solid-state batteries are packed by the external pressure. Thus, the local electro-chemical potential of the Li^+ in the SE is controlled by the Li^+ concentration, electrostatic potential and pressure, and it can be expressed as

$$\mu_{Li^+} = \mu_{Li^+}^0 + RT\ln c_+ + F\phi_{SE} + \nu_{SE}P_{SE} \tag{S1}$$

where μ_{Li+}^0 denotes the reference chemical potential of Li^+. R and T are the molar gas constant and temperature respectively. c_+ is the concentration of the Li^+ in SE. F is the Faraday's constant. ϕ_{SE} is the electrostatic potential in the SE. $v_{SE}P_{SE}$ is the mechanical potential which refers to the mechanical contribution that shifts the electrochemical potential of the SE, where v_{SE} is the molar volume of the SE (e.g., LLZO) and P_{SE} is the hydrostatic pressure. The detailed derivation of the mechanical potential can be found in our previous work[1].

Then, the flux of Li^+ in the SE can be derived from the gradient of the electrochemical potential, and it can be written as

$$\begin{aligned}\mathbf{N}_+ &= -Mc_+\nabla\mu_{Li^+} \\ &= -M\left(RT\nabla c_+ + Fc_+\nabla\phi_{SE} + \nu_{SE}c_+\nabla P_{SE}\right)\end{aligned} \tag{S2}$$

where M is the mobility of Li^+ in SE. According to the Einstein relation, it can be expressed as $MRT=D_{SE}$, where D_{SE} is the diffusion coefficient of Li^+ in SE. Thus, Li^+ diffusion equation can be expressed as

$$\frac{\partial c_+}{\partial t} = -\nabla \mathbf{N}_+ = \nabla \cdot \left(D_{SE} \nabla c_+ + \frac{D_{SE}}{RT} F c_+ \nabla \phi_{SE} + \frac{D_{SE}}{RT} \nu_{SE} c_+ \nabla P_{SE} \right) \quad \text{(S3)}$$

The electrostatic potential is governed by the Poisson equation, and expressed as

$$\nabla \cdot \sigma_{SE} \nabla \phi_{SE} = 0 \quad \text{(S4)}$$

where σ_{SE} is the ionic conductivity of Li^+ in the SE. For the deformation of SE, the mechanical response can be described as the linear elastic relationship between the elastic modulus and strain. Distributions of the mechanical stress and strain of the SE can be obtained by solving the stress equilibrium equation which can be written as

$$\nabla \cdot \boldsymbol{\sigma}_{\mathbf{s}} = 0 \quad \text{(S5)}$$

where σ_s is the stress in the SE.

S1.2 Creep stress in Li metal

Due to the strain-rate-dependent creep deformation behavior of Li metal, we suggest that Li metal could behave like an incompressible viscous fluid, where the hardness of Li metal (~MPa)[2] is much smaller than that of the SE (~GPa)[3]. Then, we introduce the fluid-structure interaction (FSI) theory to couple Li metal and SE when Li metal anode contacting the mechanically hard SE, as shown in **Figure S1**. The metal flow of the relatively soft Li is treated by using viscous creeping flow with negligible elastic strain (i.e., incompressible). The constitutive relationship of the Li metal is obtained in terms of the experimentally measured power-law creep model[4], and it can be expressed as:

$$\boldsymbol{\sigma}_{creep} = \left(\frac{\dot{\boldsymbol{\varepsilon}}_{creep}}{A_c} \right)^{1/m} \exp\left(\frac{Q_c}{mRT} \right) \quad \text{(S6)}$$

where $\boldsymbol{\sigma}_{creep}$ and $\dot{\boldsymbol{\varepsilon}}_{creep}$ are, respectively, the creep stress and the corresponding strain rate on Li deformation. A_c is a material-specific creep parameter. m is the power-law creep exponent of Li metal. Q_c is the activation energy for dislocation climb. And in the time-dependent deformation, the strain rate is defined as

$$\dot{\boldsymbol{\varepsilon}}_{creep} = \frac{1}{2}\left(\nabla \mathbf{u} + \nabla \mathbf{u}^T\right) \tag{S7}$$

where $\mathbf{u}$ is the displacement rate.

Leaving out the time dependence and the advective terms, the obtained creep flow governing equation is a steady state momentum conservation equation, and it can be expressed as

$$-\nabla P\mathbf{I} + \nabla\left(\left(\frac{\dot{\boldsymbol{\varepsilon}}_{creep}}{A_c}\right)^{1/m} \exp\left(\frac{Q_c}{mRT}\right)\right) = 0 \tag{S8}$$

And then the stress can be written as

$$\sigma_{ij} = -p\delta_{ij} + A_c^{-1/m} \exp\left(\frac{Q_c}{mRT}\right) \cdot \nabla\left(\dot{\varepsilon}_{ij}\right)^{1/m} \tag{S9}$$

where p is the effective pressure. $\mathbf{I}$ is the unit tensor in the Lagrange coordinate. δ_{ij} is the Kronecker symbol. Furthermore, by fitting the creep law (i.e., Equation S6) and treating the Li metal flow as the viscous creeping flow, then, the metal pseudo-viscosity η_{creep} is obtained. Then, the Equation S8 can be expressed as the Stokes equation with small Reynolds number (i.e., Re<<1),

$$-\nabla P^*\mathbf{I} + \eta_{creep}\nabla^2\mathbf{u} = 0 \tag{S10}$$

The Stokes equation (i.e., Equation S10) of the Li metal creep flow, is solved together with the mass transport, electrostatic Poisson's equation and stress equilibrium equations in the SE.

S1.3 Linking Li^+ transport and creep stress of Li metal

The interaction between Li metal and SE at the Li/SE interface is the most important point to couple Li metal creep flow and SE. It can be account for the electrochemical and mechanical responses in a bidirectional manner and described as the boundary terms at the Li/SE interface. On the one hand, the Li^+ diffusion equation can be solved by including the boundary condition of the diffusional potential that is a function of creep stress and electrostatic potential. The diffusion potential boundary condition can be expressed as

$$\Phi_0 = \mu_0 + V_{Li} \cdot \Delta p_{Li} \tag{S11}$$

where μ_0 is the reference electrochemical potential of Li^+ at the Li/SE interface. V_{Li} is the molar volume of Li metal. ΔP_{Li} is the hydrostatic pressure difference between the deformed and undeformed states at the contact surface of the Li metal. $V_{Li}\Delta P_{Li}$ refers to the mechanical contribution that shifts the electrochemical potential at the interface.

The diffusional potential Φ_0 can be account for the interfacial reaction kinetics which is driven by the electrochemical potential and mechanical stress during charging/discharging conditions. Considering that the mechanical stress impacts the reaction kinetics, the modified Butler-Volmer equation which is extended by Monroe and Newman[5], can be introduced

$$i = i_{exc} \exp\left(\frac{(1-\alpha_a)V_{Li}\Delta p_{Li}}{RT}\right)\left(\exp\left(\frac{\alpha_a F \eta_{tot}}{RT}\right) - \exp\left(\frac{-\alpha_c F \eta_{tot}}{RT}\right)\right) \tag{S12}$$

where i_{exc} is the reference exchange current density. The anodic and cathodic charge transfer coefficients yield $\alpha_a = 1 - \alpha$ and $\alpha_c = \alpha$, respectively, where α is an asymmetric factor varying from 0 to 1 and is set as to 0.5 in this study. η_{tot} is the total overpotential at the interface, and it can be given as $\eta_{tot}=\eta_e+v_{Li}P_{Li}/F$, where η_e is the electrochemical overpotential, and $v_{Li}P_{Li}/F$ refers to

the mechanical overpotential. The interfacial Li^+ flux is related to the local current density, and expressed as

$$\mathbf{N}_+^0 = \frac{\mathbf{i}_{\mathbf{interface}}}{F} \tag{S13}$$

where $\mathbf{i}_{\text{interface}}$ is the local current density at the Li/SE interface. And the reference exchange current density is given as[5,6]:

$$i_{exc} = F \cdot k_{ref} \cdot \left(c_+\right)^{\alpha_a} \tag{S14}$$

where k_{ref} is the reference rate of the interfacial reaction during Li stripping or Li deposition. Therefore, combing Equation S11-S14, the diffusional potential boundary condition can be replaced by the interfacial flux boundary condition, which is related to the interfacial reaction rate (stripping rate or deposition rate) and mechanical stress. It can be written as

$$R_0 = \left(c_+\right)^{\alpha_a} \cdot k_{ref} \cdot \exp\left(\frac{\left(1-\alpha_a\right)V_{Li}\Delta p_{Li}}{RT}\right)\left(\exp\left(\frac{\alpha_a F \eta_{tot}}{RT}\right) - \exp\left(\frac{-\alpha_c F \eta_{tot}}{RT}\right)\right) \tag{S15}$$

On the other hand, the interfacial strain rate depends on the interface reaction rate and external pressure, thus, the gradient of the Li^+ flux can be treated as the strain rate of the creep deformation. And the obtained creep strain rate can be used as the boundary condition for the Li metal creep flow equation. Of particular note is that the strain rate boundary condition can be expressed in terms of the metal displacement rate, i.e.,

$$\mathbf{u}_0 = \mathbf{u}_{ep} \pm \beta V_{Li} \cdot \mathbf{N}_+^0 \tag{S16}$$

where $\mathbf{u}_{ep}$ refers to the external pressure contributed interfacial displacement rate. $\mathbf{N}_+^0$ is the Li^+ flux at the Li/SE interface. + and – represent the Li deposition process and Li stripping process, respectively. β is the relative volume change between the Li metal lattice and the SE lattice, herein, it is defined as 3.5 which is the ratio of the Li metal lattice constant and LLZO lattice constant. In

addition, for Li deposition, the interfacial momentum balance should be maintained due to the well contacted interface, i.e., $\sigma_{creep}^{0} \cdot \mathbf{n} + \sigma_{s}^{0} \cdot \mathbf{n} = 0$, where $\mathbf{n}$ is the interface normal vector, σ_{creep}^{0} is the stress at the Li metal boundary and σ_{s}^{0} is the stress at the SE boundary. However, for Li dissolution, owing to the depletion of Li atoms and consequently contact loss, the aforementioned interfacial momentum balance is hardly to maintained.

Recent experiments exhibit that the size effect takes an important role in the mechanical properties (such as yield strength) and the interface stress for lithium metal. The traditionally measured yield strength is in the range of 0.6~1.26 MPa[2,4,7] from bulk testing (i.e., macroscopic samples of Li). However, for nanoindentation or micropillar testing (length scale < 100 μm), Matt Pharr et al.[2] show that the yield strength of Li varies between 6.7 and 14 MPa for the length scale of Li between 10 and 2.3 μm. Greer et al.[8] report that the yield strength of Li pillars between 10 and 100 MPa with the length scale between 10 and 1μm.

Besides the yield strength, the stress exponent and interfacial stress show the size-dependance as well. The stress exponent of bulk Li is about 6.55~6.6[2,4,7], while the nanoindentation testing shows the stress exponent value of 6.9[2]. Zhang et al.[9] report that the interfacial compressive stress varies between 10 and 130 MPa with the equivalent diameter of Li whisker between 600 and 100nm. Hence, the mechanical behavior of Li metal exhibits the significant size dependence.

However, considering that the measured yield strength and compressive stress differ significantly from one research work to another. More experimental measurements should be applied to reveal the size-dependence on Li metal. Therefore, our work is not included the size-dependence on the mechanical behavior of Li metal. Since our simulation is at microscale the yield strength we used is 14 MPa, obtained from Zhang[10] whose analysis suggests that a reasonable estimation of the Li yield strength is 16 ± 2 MPa at microscale.

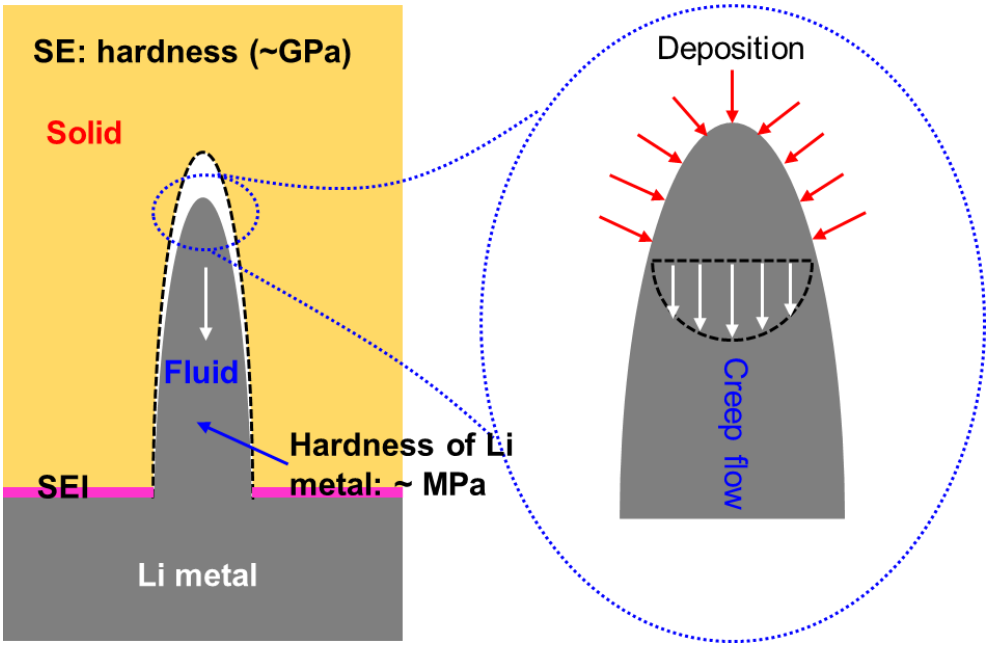

Figure S1. Hypothesis: analogy of Li/SE interaction to fluid-structure interaction due to the strain-rate dependent creep deformation mechanism of Li metal.

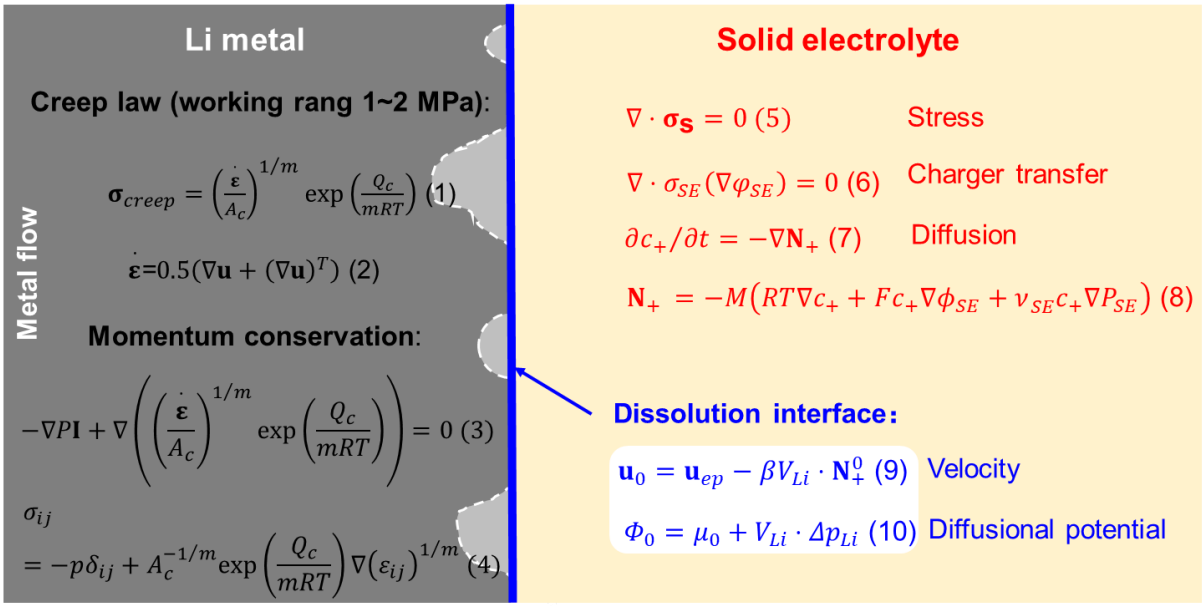

Figure S2. Governing equations of the creep/contact model and boundary terms to couple Li metal and SE at the Li/SE interface.

S2. Calculation of $J_{diffusion}$

This section presents the detailed procedure to calculate the maximum concentration of vacancies at an ideal flat Li/SE interface which is an important input to compute $J_{diffusion}$, as given in the follow:

$$J_{diffusion} = \left(1 - \frac{c_{vac}}{c_{vac}^0}\right) c_{vac}^0 \sqrt{\frac{D_{vac}}{\tau_{vac}}} \quad \text{(S17)}$$

where c_{vac} is the maximum value of the concentration of the vacancies at the Li/SE interface which depends on the current density during stripping[11–13]. c_{vac}^0 is the equilibrium concentration of Li vacancies, and is approximately $8\text{x}10^{-9}$ mol/cm^3 which are estimated by ab initio calculations[14]. D_{vac} is the diffusion coefficient of Li vacancies and is around 10^{-10} cm^2/s at room temperature[15–17]. τ_{vac} is the relaxation time of Li vacancies, which is assumed to be approximately 5 s[18]

Herein, we perform the one-dimensional (1D) creep/contact model with an ideal flat Li/SE interface to calculate the Li^+ concentration which can be used to estimate the maximum concentration of vacancies, as shown in **Figure S3**. In principle, for the Li stripping process, a Li atom at the surface of Li metal lost the electron, and consequently producing a Li^+. The produced Li^+ passes the Li/SE interface and toward the bulk LLZO, leaving an electron and a vacant site in the surface of Li metal. Thus, the number of generated vacancies is equivalent to that of the produced Li^+. Therefore, we can use the interfacial Li^+ concentration to simply estimate the maximum concentration of vacancies at an ideal flat Li/SE interface. By performing the 1D creep/contact model, the calculated interfacial Li^+ concentration (captured at 2000s at which the equilibrium is almost achieved, see Figure S3a) is used as the maximum concentration of vacancies at the interface i.e., $c_{vac} = c_+$ (t=2000 s), as shown in Figure S3b.

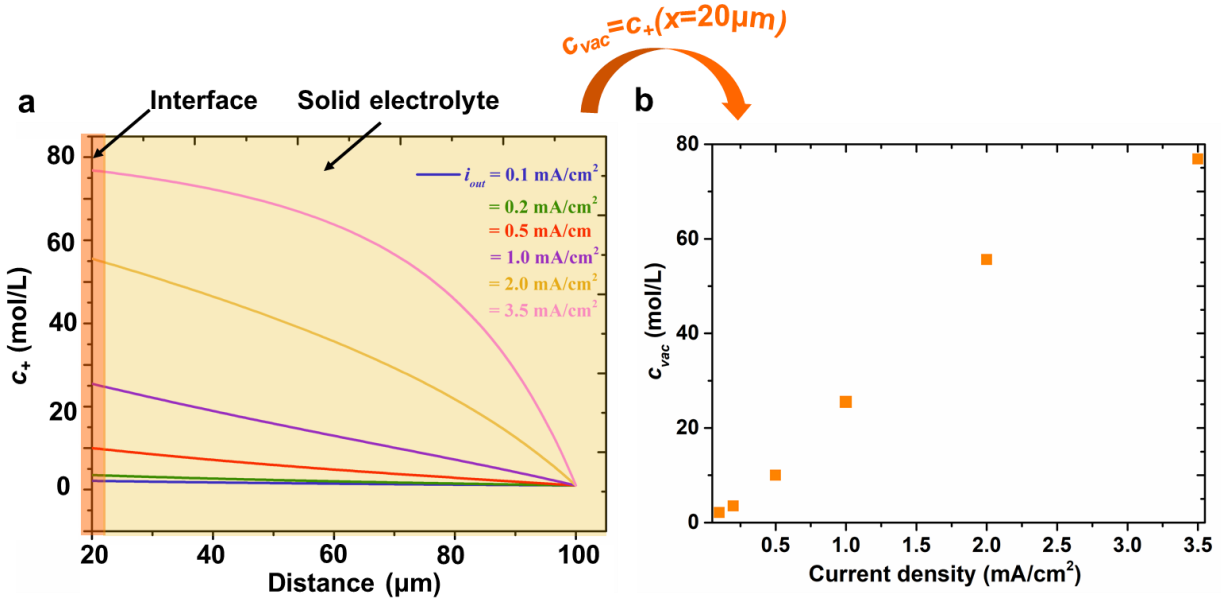

Figure S3. (**a**) Distribution of the Li^+ concentration in SE as a function of current density under a stack pressure of 3 MPa. (**b**) The maximum concentration of vacancies (c_{vac}) at an ideal flat interface as a function of current density.

S3. Validation of the creep/contact model and calibration of J_{creep} and $J_{diffusion}$

This section presents the detailed procedure to validate the developed creep/contact model and calibrate J_{creep} and $J_{diffusion}$. Firstly, several simulations are performed to validate the model. The initial and boundary conditions are shown in **Figure S5**. All simulation parameters are listed in Table S1. **Figure 2e** shows the calculated compressive stress at the Li/SE interface as a function of stack pressure together with the experimental and simulation reported results. It is observed that the calculated compressive stress is in the range from 1 to 15 MPa when subjected to a stack pressure from 1 to 15 MPa. Although recent experimental measured and simulation calculated Li stress differs vastly from one to another, the magnitude of the Li stress is in the range from 3 to 1000 MPa[9,10,19–21]. And our calculated Li stress generally falls in the reasonable range of those reported values.

Then, J_{creep} and $J_{diffusion}$ is calibrated by using the experimental reported results. According to recent experimental measurements[22,23], the critical stack pressures of preventing void formation are 0.4, 2, 3 and 7 MPa in the Li-SE systems during stripping, under the condition of the applied current densities of 0.1, 0.4, 0.2 and 1.0 mA/cm^2, respectively. Based on above, we can estimate that $J_{creep} \approx J_{migration}$, thus, the corresponding J_{creep} is 1.04x10^{-3}, 4.15x10^{-3}, 2.08x10^{-3} and 0.01 μmol/(cm^2 s). So, we determined J_{creep} values by changing the value of j_0 and λ until J_{creep} generally agrees with those experimental results, as depicted in Figure 2f. The calibrated j_0 and λ are 0.0025 μmol/(cm^2 s) and 44.17 respectively. In addition, λ is related to the creep deformation-induced dislocation density of Li metal. j_0 is the flux of the vacancy transported away from the interface without pressure, in other words, $J_{diffusion}$ is equal to j_0 at the scenario of no-ideal Li/SE interface with pre-existing defects and is 0.0025 μmol/(cm^2 s).

S4. Effect of the pre-existing interfacial defects on the vacancy concentration

This section presents the detailed simulation procedure to explore the effect of the pre-existing interfacial defects on the vacancy concentration. The governing equation of the vacancy diffusion can be expressed as

$$\frac{\partial c_{vac}}{\partial t} = \nabla \cdot D_{vac} \nabla c_{vac} + R_v \quad \text{(S18)}$$

where R_v is the generation (or trapped) rate, $R_{vacancy}$ (or R_{trap}), of the vacancies at the interface (or pre-existing defects surface).

To obtain the distribution of the interfacial vacancy concentration, the vacancy diffusion model is performed at the ideal flat Li/SE interface and non-ideal Li/SE interface (with pre-existing defects), respectively. **Figure S4**a and S4b show the initial and boundary conditions of the simulations. The initial vacancy concentration, $c_{vac}(t=0)$ is set as 8×10^{-9} mol/cm^3 which is the equilibrium concentration of the vacancies and estimated by ab initio calculations[14]. The Dirichlet boundary is applied at the left side of the Li metal with the vacancy concentration of 8×10^{-9} mol/cm^3. The Neumann boundary is applied at the Li/SE interface with the generation rate of the vacancies, $R_{vacancy}$ =3.94x10^{-4} μmol/(cm^2 s), which is approximately to the generation rate of Li^+ at the current density of 0.1 mA/cm^2. While for the surface of the pre-existing defects, the Neumann boundary is applied with the trapped/absorption rate of the vacancies, R_{trap}=-1.97x10^{-4} μmol/(cm^2 s), which is careful chosen and calibrated to keep the $J_{diffusion}$ (calibrated in Supporting Information S3) approximately the value of 0.0025 μmol/(cm^2 s). As observed in Figure S4c and S4d, the interfacial vacancy concentration is remarkable decreased at the non-ideal interface with pre-existing defects, comparing to that at the ideal flat interface. This confirms that the maximum

concentration of the vacancy is reduced at the non-ideal Li/SE interface due to the pre-existing defects.

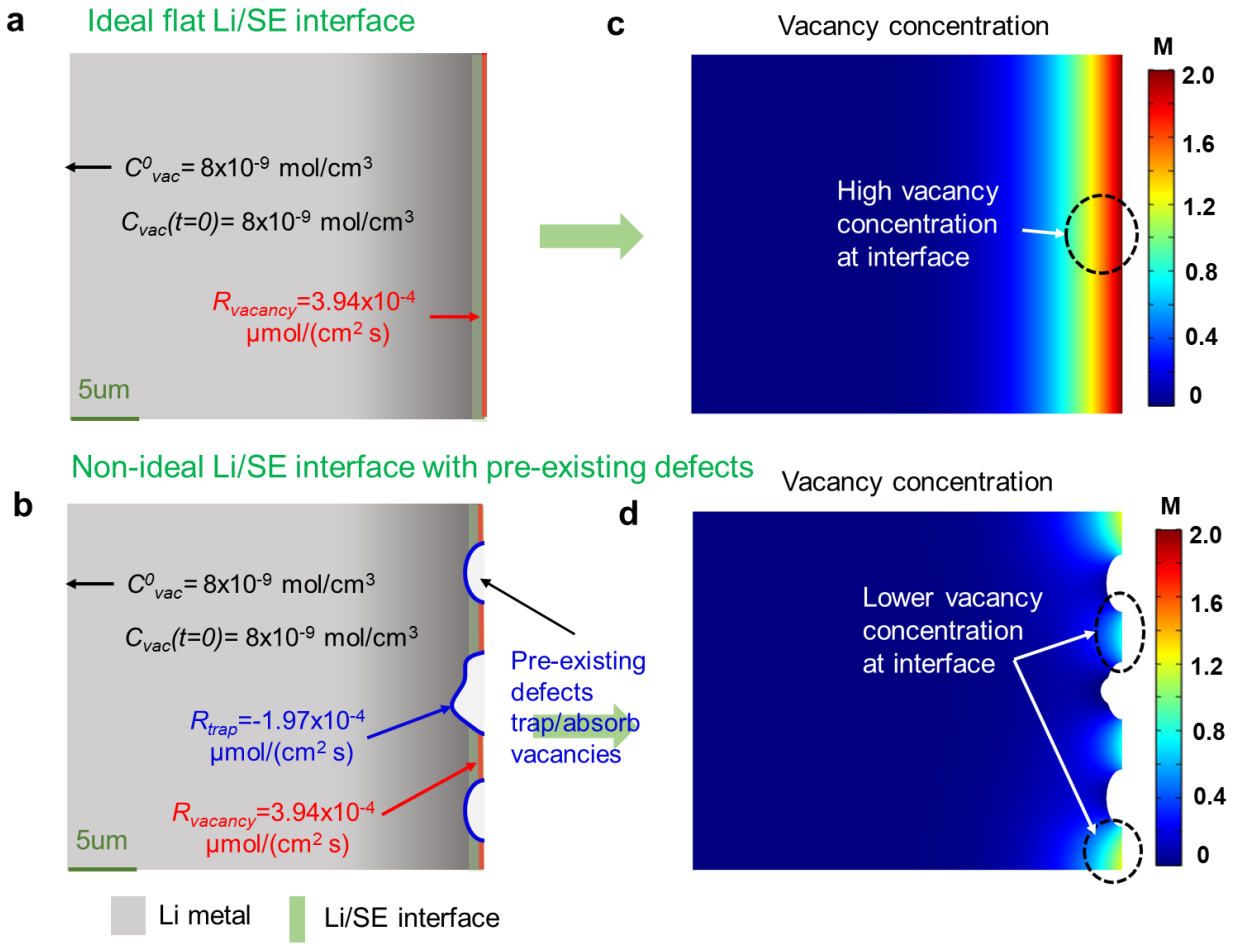

Figure S4. The geometry and initial and boundary conditions of the vacancy diffusion at the case of (**a**) ideal flat Li/SE interface and (**b**) non-ideal Li/SE interface with pre-existing defects, and the corresponding vacancy concentration profile is shown in (**c**) and (**d**) respectively.

S5. Simulation details for 1D creep/contact model

This section presents the simulation details of the 1D creep/contact model. The simulation is carried out in COMSOL Multiphysics 5.4, employing the finite element methods. The model involves four governing equations: Equation S3-S5 and S10, which governs Li^+ concentration (c_+), electric field (ϕ_{SE}), stress distribution of SE and creep flow stress of Li metal, respectively. Figure S5 illustrates the geometry and initial and boundary conditions for all equations. The thickness of Li metal and SE are set as 20 and 60 μm, respectively. We set the initial electric potential in the SE is 0 V, and the initial Li^+ concentration in the SE is 1 mol/L. The initial stress and displacement in both Li metal and SE domains are zero. The Dirichlet boundary and Neumann condition are applied at the opposite side of SE with the Li^+ concentration of 1 mol/L and the output current density i_{out}, respectively. And the left boundaries of SE are subjected to Equation S12 and S15, respectively. In mechanics part, for SE, the right boundary is fixed, and the left boundary is subjected to either fixed displacement or stack pressure. For Li metal, the left boundary is fixed, and the right boundary is subjected to Equation S16. The other model parameters are listed in Table S1.

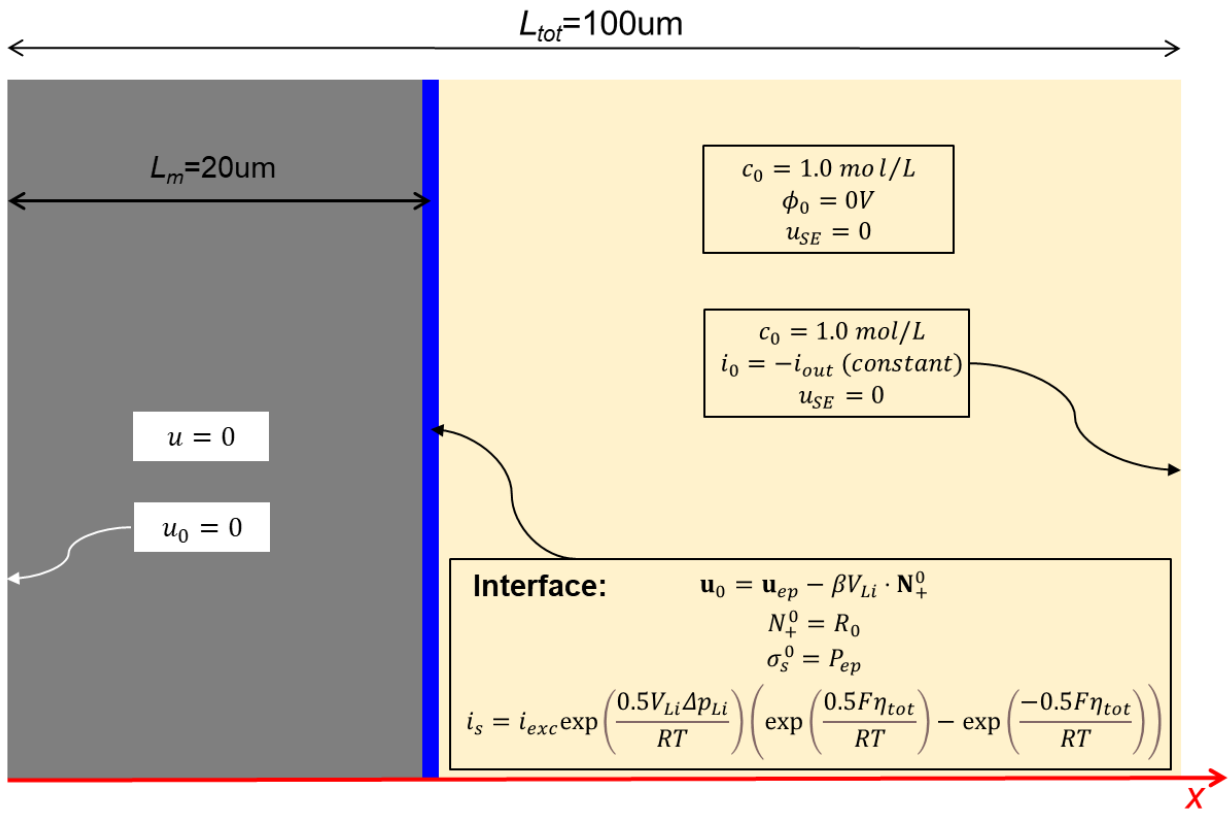

Figure S5. The geometry and initial and boundary conditions of the 1D creep/contact model.

S6. Simulation details for 2D creep/contact model

In this section, the simulation details of the 2D creep/contact model are presented. Similarly, simulations are performed in COMSOL Multiphysics 5.4, which based on finite element method. The tetrahedral mesh is applied and fined enough near the pore region such that the calculations are run smoothly. The model involves four governing equations, i.e., Equation S3-S5 and S10. **Figure S6** shows the geometry and initial and boundary conditions for all equations. The domain size is 80 x 40 μm. The initial pore is located at the center of the Li/SE interface. The thickness of Li metal and SE is 20 and 60 μm, respectively. The details of the initial and boundary conditions are similar to the previous section. The Neumann boundaries or roller boundaries are applied at the top and bottom of both Li metal and SE. In addition, due to the weakly impact of the mechanical stress on the mass transport, in mechanical part, the left boundary of the SE is only applied a constant pressure in the range from 1 to 5 MPa. The others model parameters are listed in Table S1.

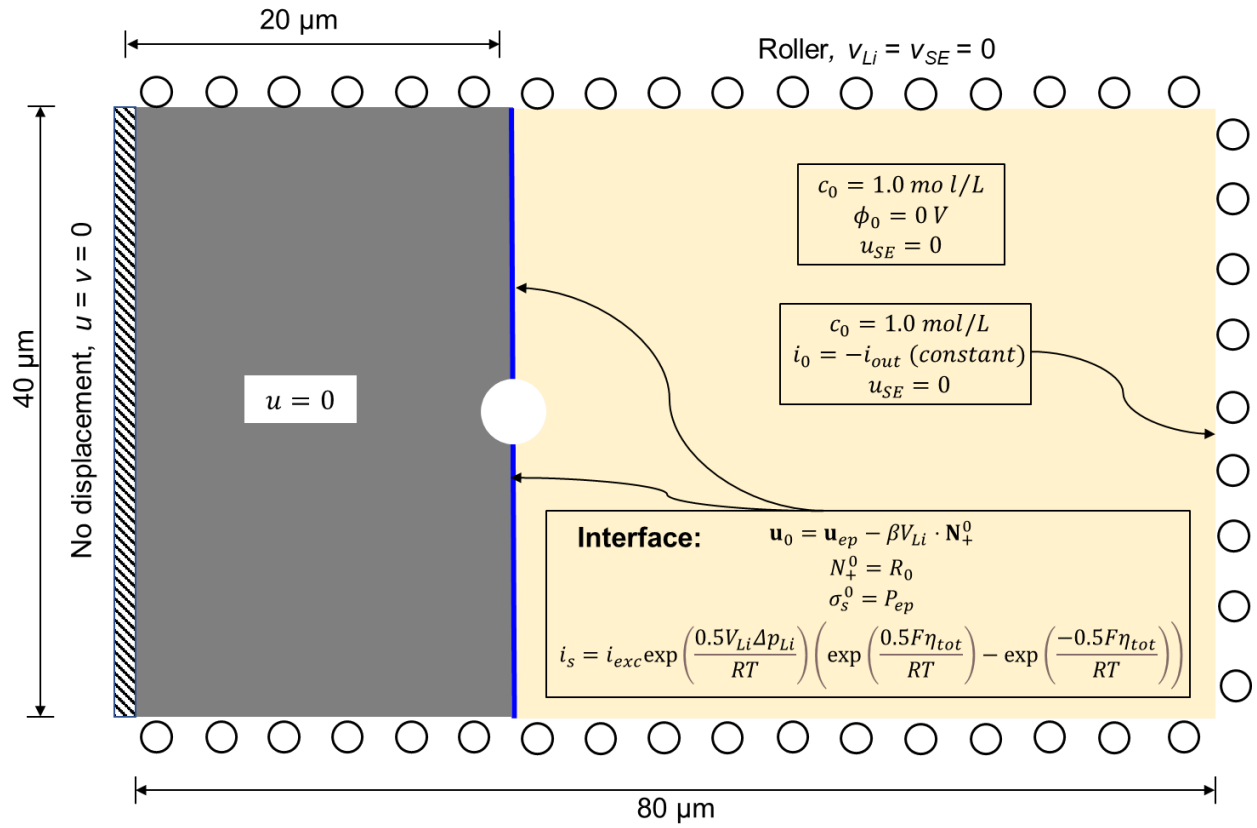

Figure S6. The geometry and initial and boundary conditions of the 2D creep/contact model.

S7. Selection of L_χ

This section presents the selection details of L_χ. To reveal the local effect of the pores, two parameters (i.e., local impact factor χ and local length in y direction L_χ) are introduced. Herein, the local impactor factor is defined as

$$\chi = \frac{i_{local}}{i_{average}} \tag{S19}$$

where $i_{average}$ is the average current density at the Li/SE interface. i_{local} is the current density at the Li/SE interface. And the local length in y direction, L_χ is defined when the χ is away from 1.

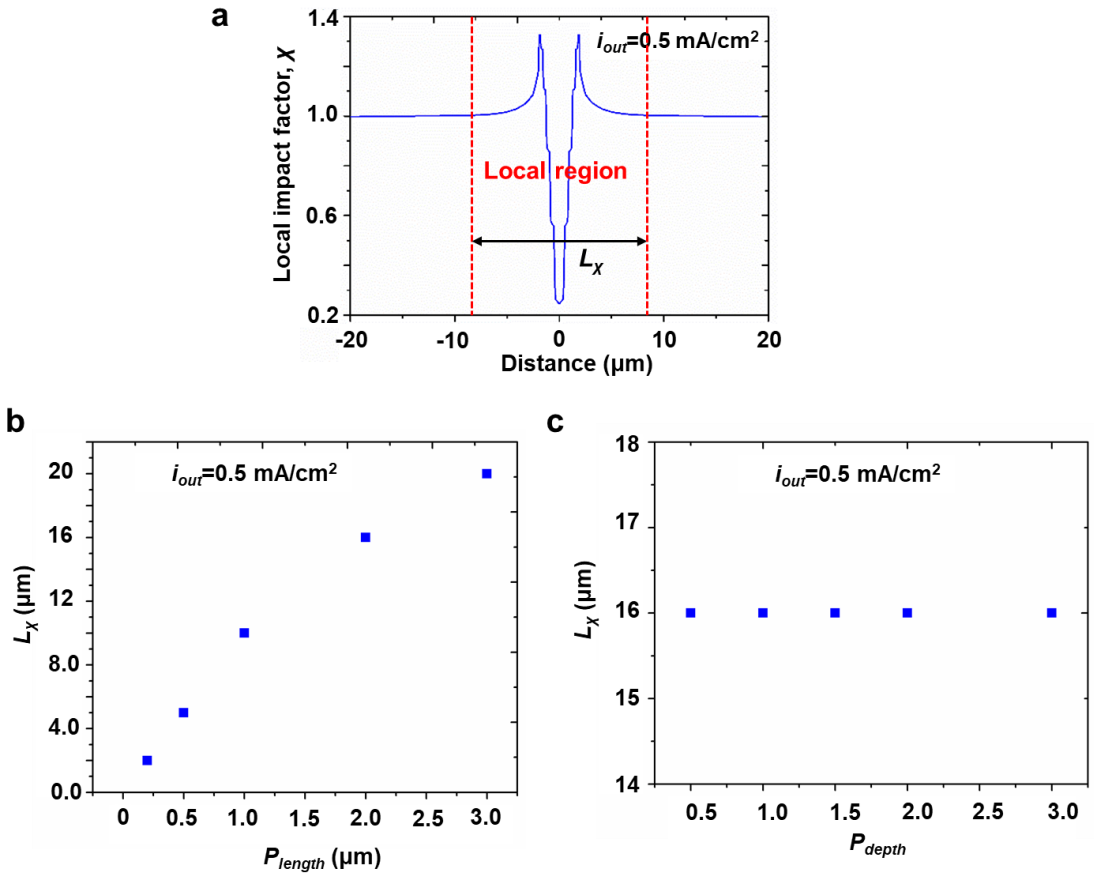

Figure S7. (**a**) Schematic diagram of the definition of the local region and local length L_χ in y-axis direction. The selected L_χ in the y-axis direction as a function of the (**b**) pore length P_{length} and (**c**) pore depth P_{depth}, respectively.

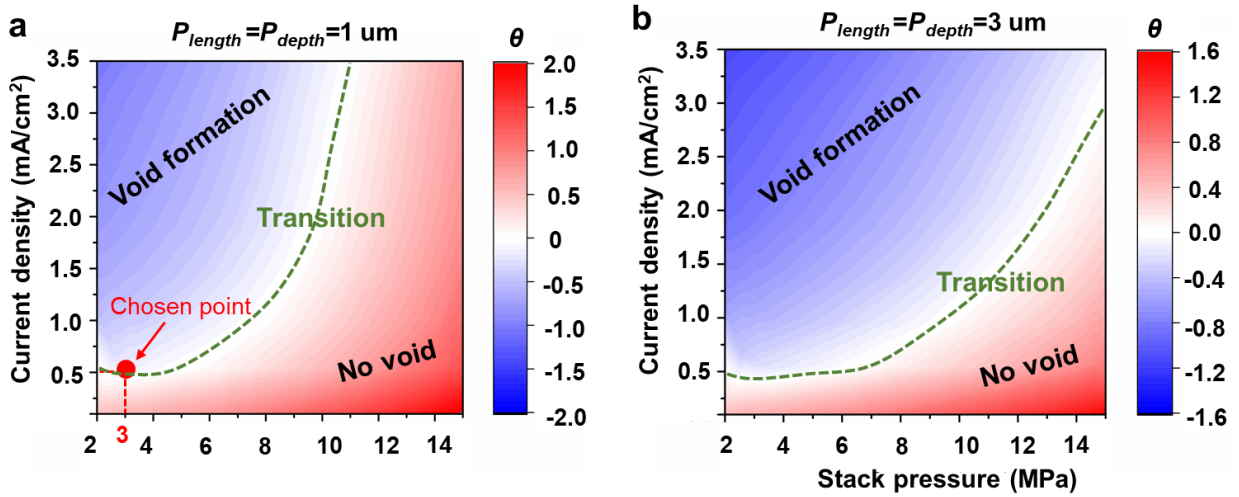

Figure S8. A map of void formation as a function of stack pressure and current density with P_{length}=P_{depth} of (**a**) 1 μm and (**b**) 3 μm respectively. The red circle is the chosen point which is located near the critical lines with the corresponding stack pressure of 3MPa and current density of 0.5 mA/cm^2.

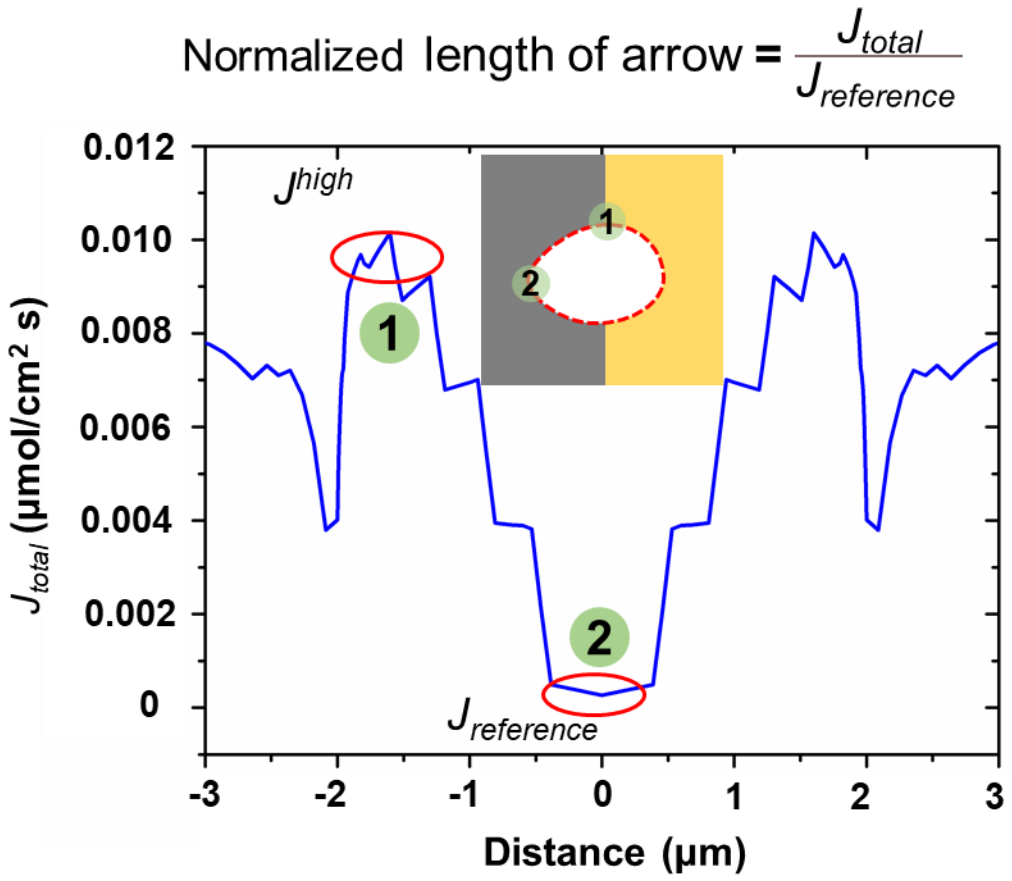

Figure S9. The simulated distribution of J_{total} along the pore edges under the current density of 1.0 mA/cm^2 and stack pressure of 3 MPa with P_{length}=P_{depth} =2 μm.

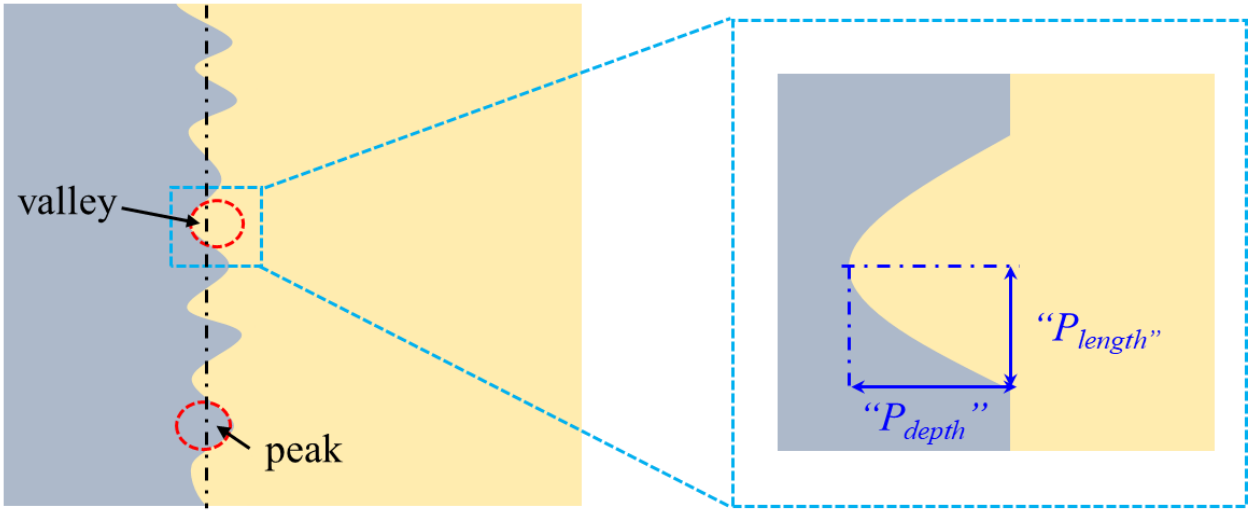

Figure S10. Schematics of the linking between surface roughness and pore dimensions (i.e., P_{depth} and P_{length}).

Table S1. Model parameters in the simulations of the creep/contact model during stripping.

	Symbol	Unit	Real value	reference
		Li metal		
Material-specific creep parameter	$A_c^{-1/m}$	Pa/s	3.0×10^5	[4]
Power-law creep exponent	m	/	6.6	[4]
Activation energy	Q_c	J/mol	3.7×10^4	[4]
Fcc-Li molar volume	v_{Li}	m^3/mol	12.9×10^{-6}	[24]
Bulk concentration of Li^+	c_{bulk}	mol/m^3	42.6×10^3	[25]
		LLZO		
Elastic modulus of LLZO	E_{SE}	Pa	150×10^9	[26]
LLZO molar volume	v_{SE}	m^3/mol	165×10^{-6}	[27]
Li^+ diffusion coefficient in LLZO	D_{SE}	m^2/s	1.4×10^{-12}	[28,29]
Ionic conductivity of Li^+ in LLZO	σ_{SE}	mS/cm	0.26	[30]
Exchange current density of LLZO	i_{exc}	$\mu A/cm^2$	240	[30]
		System		
Initial Li^+ concentrations	c_0	mol/m^3	1000	/
Temperature	T	K	298	/
Reference reaction rate	k_{ref}	$mol^{0.5}/(m^{0.5}\,s)$	1.375×10^{-6}	/
Reference $J_{diffusion}$	j_0	$\mu mol/(cm^2\,s)$	0.0025	/
Dislocation-related constant	λ	/	44.174	/

References

[1] K. Tantratian, H. Yan, K. Ellwood, E. T. Harrison, L. Chen, **n.d.**, DOI 10.1002/aenm.202003417.

[2] C. D. Fincher, D. Ojeda, Y. Zhang, G. M. Pharr, M. Pharr, *Acta Mater.* **2020**, DOI 10.1016/j.actamat.2019.12.036.

[3] J. Wolfenstine, J. L. Allen, J. Sakamoto, D. J. Siegel, H. Choe, *Ionics (Kiel).* **2018**, DOI 10.1007/s11581-017-2314-4.

[4] W. S. LePage, Y. Chen, E. Kazyak, K. H. Chen, A. J. Sanchez, A. Poli, E. M. Arruda, M. D. Thouless, N. P. Dasgupta, *J. Electrochem. Soc.* **2019**, DOI 10.1149/2.0221902jes.

[5] C. Monroe, J. Newman, *J. Electrochem. Soc.* **2004**, DOI 10.1149/1.1710893.

[6] P. Barai, A. T. Ngo, B. Narayanan, K. Higa, L. A. Curtiss, V. Srinivasan, *J. Electrochem. Soc.* **2020**, *167*, 100537.

[7] A. Masias, N. Felten, R. Garcia-Mendez, J. Wolfenstine, J. Sakamoto, *J. Mater. Sci.* **2019**, DOI 10.1007/s10853-018-2971-3.

[8] C. Xu, Z. Ahmad, A. Aryanfar, V. Viswanathan, J. R. Greer, *Proc. Natl. Acad. Sci. U. S. A.* **2017**, DOI 10.1073/pnas.1615733114.

[9] L. Zhang, T. Yang, C. Du, Q. Liu, Y. Tang, J. Zhao, B. Wang, T. Chen, Y. Sun, P. Jia, H. Li, L. Geng, J. Chen, H. Ye, Z. Wang, Y. Li, H. Sun, X. Li, Q. Dai, Y. Tang, Q. Peng, T. Shen, S. Zhang, T. Zhu, J. Huang, *Nat. Nanotechnol.* **2020**, DOI 10.1038/s41565-019-0604-x.

[10] X. Zhang, Q. J. Wang, K. L. Harrison, S. A. Roberts, S. J. Harris, *Cell Reports Phys. Sci.* **2020**, *1*, 100012.

[11] F. Shi, A. Pei, D. T. Boyle, J. Xie, X. Yu, X. Zhang, Y. Cui, *Proc. Natl. Acad. Sci. U. S.*

A. **2018**, DOI 10.1073/pnas.1806878115.

[12] M. Yang, Y. Liu, A. M. Nolan, Y. Mo, *Adv. Mater.* **2021**, DOI 10.1002/adma.202008081.

[13] Y. T. Chiu, K. L. Lin, Y. S. Lai, *J. Appl. Phys.* **2012**, DOI 10.1063/1.3682480.

[14] W. Frank, U. Breier, C. Elsässer, M. Fähnle, *Phys. Rev. Lett.* **1996**, DOI 10.1103/PhysRevLett.77.518.

[15] T. R. Jow, C. C. Liang, *J. Electrochem. Soc.* **1983**, *130*, 737.

[16] R. Messer, F. Noack, *Appl. Phys.* **1975**, DOI 10.1007/BF00883553.

[17] E. Dologlou, *Glas. Phys. Chem.* **2010**, DOI 10.1134/S1087659610050056.

[18] T. Krauskopf, H. Hartmann, W. G. Zeier, J. Janek, *ACS Appl. Mater. Interfaces* **2019**, *11*, 14463.

[19] Y. Chen, Z. Wang, X. Li, X. Yao, C. Wang, Y. Li, W. Xue, D. Yu, S. Y. Kim, F. Yang, A. Kushima, G. Zhang, H. Huang, N. Wu, Y. W. Mai, J. B. Goodenough, J. Li, *Nature* **2020**, *578*, 251.

[20] Y. He, X. Ren, Y. Xu, M. H. Engelhard, X. Li, J. Xiao, J. Liu, J. G. Zhang, W. Xu, C. Wang, *Nat. Nanotechnol.* **2019**, DOI 10.1038/s41565-019-0558-z.

[21] Q. Tu, L. Barroso-Luque, T. Shi, G. Ceder, *Cell Reports Phys. Sci.* **2020**, *1*, 100106.

[22] M. J. Wang, R. Choudhury, J. Sakamoto, *Joule* **2019**, DOI 10.1016/j.joule.2019.06.017.

[23] J. Kasemchainan, S. Zekoll, D. Spencer Jolly, Z. Ning, G. O. Hartley, J. Marrow, P. G. Bruce, *Nat. Mater.* **2019**, DOI 10.1038/s41563-019-0438-9.

[24] B. Hallstedt, *Calphad Comput. Coupling Phase Diagrams Thermochem.* **2007**, DOI 10.1016/j.calphad.2006.10.006.

[25] H. Xie, J. A. Alonso, Y. Li, M. T. Fernández-Díaz, J. B. Goodenough, *Chem. Mater.* **2011**, DOI 10.1021/cm201671k.

[26] S. Yu, R. D. Schmidt, R. Garcia-Mendez, E. Herbert, N. J. Dudney, J. B. Wolfenstine, J. Sakamoto, D. J. Siegel, *Chem. Mater*. **2016**, DOI 10.1021/acs.chemmater.5b03854.

[27] E. A. Il'ina, A. A. Raskovalov, O. G. Reznitskikh, *J. Chem. Thermodyn.* **2019**, DOI 10.1016/j.jct.2018.08.009.

[28] K. Hayamizu, Y. Terada, K. Kataoka, J. Akimoto, T. Haishi, *Phys. Chem. Chem. Phys.* **2019**, *21*, 23589.

[29] K. Hayamizu, Y. Terada, K. Kataoka, J. Akimoto, *J. Chem. Phys.* **2019**, DOI 10.1063/1.5089576.

[30] H. Buschmann, S. Berendts, B. Mogwitz, J. Janek, *J. Power Sources* **2012**, DOI 10.1016/j.jpowsour.2012.01.094.